Atmos. Chem. Phys., 8, 6823–6838, 2008
www.atmos-chem-phys.net/8/6823/2008/

Atmospheric Chemistry and Physics

Measurements of HNO_3 and N_2O_5 using ion drift-chemical ionization mass spectrometry during the MILAGRO/MCMA-2006 campaign

J. Zheng[1], R. Zhang[1], E. C. Fortner[1,*], R. M. Volkamer[2,3], L. Molina[2], A. C. Aiken[3,4], J. L. Jimenez[3,4], K. Gaeggeler[5], J. Dommen[5], S. Dusanter[6], P. S. Stevens[6], and X. Tie[7]

[1]Dept. of Atmospheric Sciences, Texas A&M University, College Station, Texas 77843, USA
[2]Molina Center for Energy and the Environment, La Jolla, California and Massachusetts Institute of Technology, Cambridge, Massachusetts, USA
[3]Dept. of Chemistry and Biochemistry, University of Colorado at Boulder, Boulder CO, USA
[4]Cooperative Institute for Research in the Environmental Sciences (CIRES), University of Colorado, Boulder, Colorado, USA
[5]Laboratory of Atmospheric Chemistry, Paul Scherrer Institute, Switzerland
[6]Dept. of Chemistry, Indiana University, Bloomington, Indiana, USA
[7]Atmospheric Chemistry Division, National Center for Atmospheric Research, Boulder, Colorado, USA
[*]now at: Dept. of Chemistry and Biochemistry, Montana State University, Bozeman, Montana, USA

Received: 18 January 2008 – Published in Atmos. Chem. Phys. Discuss.: 6 March 2008
Revised: 1 September 2008 – Accepted: 7 October 2008 – Published: 28 November 2008

Abstract. An ion drift-chemical ionization mass spectrometer (ID-CIMS) was deployed in Mexico City between 7 and 31 March to measure gas-phase nitric acid (HNO_3) and dinitrogen pentoxide (N_2O_5) during the Mexico City Metropolitan Area (MCMA)-2006 field campaign. The observation site was located at the Instituto Mexicano del Petróleo in the northern part of Mexico City urban area with major emissions of pollutants from residential, vehicular and industrial sources. Diurnally, HNO_3 was less than 200 parts per trillion (ppt) during the night and early morning. The concentration of HNO_3 increased steadily from around 09:00 a.m. central standard time (CST), reached a peak value of 0.5 to 3 parts per billion (ppb) in the early afternoon, and then declined sharply to less than half of the peak value near 05:00 p.m. CST. An inter-comparison between the ID-CIMS and an ion chromatograph/mass spectrometer (ICMS) showed a good agreement between the two HNO_3 measurements (R^2=0.75). The HNO_3 mixing ratio was found to anti-correlate with submicron-sized aerosol nitrate, suggesting that the gas-particle partitioning process was a major factor in determining the gaseous HNO_3 concentration. Losses by irreversible reactions with mineral dust and via dry deposition also could be important at this site. Most of the times during the MCMA 2006 field campaign, N_2O_5 was found to be below the detection limit (about 30 ppt for a 10 s integration time) of the ID-CIMS, because of high NO mixing ratio at the surface (>100 ppb) during the night. An exception occurred on 26 March 2006, when about 40 ppt N_2O_5 was observed during the late afternoon and early evening hours under cloudy conditions before the build-up of NO at the surface site. The results revealed that during the MCMA-2006 field campaign HNO_3 was primarily produced from the reaction of OH with NO_2 and regulated by gas/particle transfer and dry deposition. The production of HNO_3 from N_2O_5 hydrolysis during the nighttime was small because of high NO and low O_3 concentrations near the surface.

Correspondence to: R. Zhang
(zhang@ariel.met.tamu.edu)

1 Introduction

For decades, the Mexico City Metropolitan Area (MCMA), one of the largest megacities in the world, has suffered from poor air quality, particularly high concentrations of ozone (O_3) and particulate matter (Molina and Molina, 2002; Molina et al., 2007). As the home of about 20 million residents, over 4 million vehicles, and more than 45 000

industries, the MCMA emits annually near 180 kilotons (10^3 metric tons) of nitrogen oxides (NO_x=NO+NO_2), 6.7 kilotons of sulfur dioxide (SO_2), and 532 kilotons of volatile organic compounds (VOCs) into the atmosphere (CAM, 2006). Furthermore, the unique combination of geographical conditions, i.e., a basin topography, intense tropical solar radiation (19°25′ N and 99°10′ W), and high elevation (2240 m above mean sea level), makes air pollutants easier to accumulate in the MCMA and is favorable for photochemical production of O_3 and aerosols (Molina and Molina, 2002; Zhang et al., 2004a; Salcedo et al., 2006; Volkamer et al., 2006). During the late 1980s and early 1990s, this region annually experienced an hourly average O_3 concentration higher than 110 ppb on over 80% of days and the peak O_3 concentration exceeded 300 ppb on over 10% of days (Molina and Molina, 2002). The air quality has improved significantly recently due to control strategies implemented by the Mexican government authorities (Molina and Molina, 2004; Molina et al., 2008).

During the MCMA-2006 field study, a component of the MILAGRO Campaign (Molina et al., 2008), daytime O_3 at the urban site was frequently higher than 100 ppb and decreased to a few ppb at night due to a large amount of fresh NO_x emissions, resulting in a daily average NO_x concentration of over 100 ppb. Both VOCs and NO_x play critical roles in the O_3 formation in the troposphere (Finlayson-Pitts and Pitts, 1999; Tie et al., 2001; Zhang et al., 2003). Depending on the concentrations of VOCs and NO_x, O_3 production rate can be either NO_x-sensitive or VOC-sensitive (Sillman, 1999; Lei et al., 2004; Zhang et al., 2004b). Recent chemical transport model simulations suggested that the O_3 formation in the MCMA was VOC-limited (Lei et al., 2007; Tie et al., 2007). The lifecycle of NO_x and its budget in the MCMA represents one of the critical pieces of information that is required to develop effective O_3 control strategies (Lei et al., 2007). The dominant daytime sink of NO_x is through the oxidation of NO_2 by the hydroxyl radical (OH) to form nitric acid (HNO_3).

$$NO_2+OH+M\rightarrow HNO_3+M \quad \text{(R1)}$$

Nitric acid is removed from the atmosphere by dry and wet depositions (Finlayson-Pitts and Pitts, 1999). Generally, HNO_3 deposition is considered to be an irreversible sink of NO_x, but recent studies have suggested that HNO_3 deposited on the surface can be recycled back into the atmosphere as NO_x by heterogeneous reactions with NO. For example, Saliba et al. (2001) proposed that HNO_3 on the surface reacts with NO to form NO_2 and nitrous acid (HONO).

$$HNO_{3(surface)}+NO\rightarrow NO_2+HONO_{(surface)} \quad \text{(R2)}$$

Further reaction between HONO and HNO_3 forms NO_2

$$HNO_{3(surface)}+HONO_{(surface)}\rightarrow 2NO_2+H_2O_{(surface)} \quad \text{(R3)}$$

or between two HONO molecules forms NO and NO_2,

$$2HONO_{(surface)}\rightarrow NO+NO_2+H_2O_{(surface)} \quad \text{(R4)}$$

Moreover, Ramazan et al. (2006) suggested that $HNO_3{\cdot}H_2O$ complex could be photolyzed, forming HONO or NO.

$$HNO_3{\cdot}H_2O+h\nu\rightarrow HONO+H_2O_2 \quad \text{(R5)}$$

$$HNO_3{\cdot}H_2O+h\nu\rightarrow HONO\times H_2O+O \quad \text{(R6)}$$

$$HNO_3{\cdot}H_2O+h\nu\rightarrow NO\times H_2O+HO_2 \quad \text{(R7)}$$

Thus, under certain meteorological conditions, a HNO_3 enriched plume can potentially contribute to O_3 production far away from its origin.

At nighttime, NO_x reacts with O_3 to form the nitrate radical (NO_3), which further reacts reversibly with NO_2 to form dinitrogen pentoxide (N_2O_5) (for Reaction 10, $K_{eq}=2.7\times10^{-27}\exp[11000/T]\,cm^3\,molecule^{-1}$, JPL 2006).

$$NO+O_3\rightarrow NO_2+O_2 \quad \text{(R8)}$$

$$NO_2+O_3\rightarrow NO_3+O_2 \quad \text{(R9)}$$

$$NO_2+NO_3\leftrightarrow N_2O_5 \quad \text{(R10)}$$

At night, NO_3 can exist in significant concentrations and initiate H-atom abstraction or addition reactions with hydrocarbons in a similar way as OH radicals during daytime (Suh et al., 2001). Compared to NO_3, N_2O_5 is relatively unreactive in the gas-phase but undergoes heterogeneous hydrolysis reaction to form HNO_3 (Zhang et al., 1995; Brown et al., 2006).

$$N_2O_5+H_2O(l)\rightarrow 2HNO_3 \quad \text{(R11)}$$

Recent laboratory studies also suggested that NO_3 and N_2O_5 could also react with soot to produce NO_x, providing another possible pathway of renoxification (Karagulian and Rossi, 2007). Therefore, in situ observations of HNO_3 and N_2O_5 are important to fully characterize the NO_x chemistry and budget in the troposphere and to develop effective control strategies.

Several analytical techniques have been developed to measure gaseous HNO_3 in the troposphere, including nylon filter (Anlauf et al., 1988), mist chamber (Talbot et al., 1990), denuder technique (Perrino et al., 1990; Simon et al., 1995), luminol method (Hering et al., 1988), tunable diode laser spectroscopy (Horii et al., 2006), and chemical ionization mass spectrometry (CIMS) (Huey et al., 1998). Among the different approaches, the CIMS technique has the advantages of high sensitivity and fast time-response (Huey, 2007). The ion drift-chemical ionization mass spectrometry (ID-CIMS) (Fortner et al., 2004) has several additional advantages compared to the traditional CIMS technique. First,

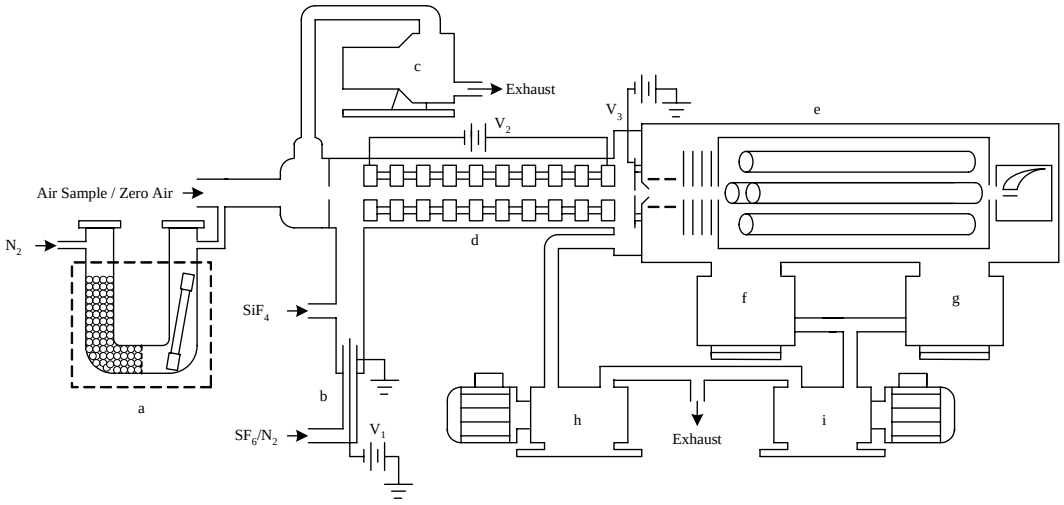

Fig. 1. Schematic diagram of the ID-CIMS: **(a)**, HNO_3 permeation device; **(b)**, ion source; **(c)**, dry scroll pump for air sampling; **(d)**, 10-ring drift tube; **(e)**, Extrel 150-QC mass spectrometer; **(f)** and **(g)**, Varian VT-551 turbo pumps; **(h)**, Edwards E2M30 oil pump; **(i)**, Varian DS402 oil pump.

a drift tube acts as ion optics (Einzel lens) to focus ions and improves the instrument sensitivity. Second, the electric field inside the drift tube guides the ion trajectory and controls the ion-molecule reaction time so that species can be quantified through kinetic calculations. Third, the presence of an appropriate electric field can inhibit formation of ion clusters inside the drift tube by collisions with carrier gas molecules.

The ambient HNO_3 mixing ratio varies considerably temporally and spatially, with reported values ranging from a few tens of ppt in clean remote environment to tens of ppb in aged urban plumes (Furutani and Akimoto, 2002; Huey et al., 2004). Despite the importance of N_2O_5 in the nocturnal NO_x chemistry, in situ N_2O_5 measurements have become possible only recently. Measurements of N_2O_5 have been performed by using cavity ring-down spectroscopy (CRDS) (Brown et al., 2002) and the CIMS technique (Huey et al., 1995). The measured N_2O_5 concentrations range from a few ppt to several hundreds of ppt (Brown et al., 2001; 2006; Slusher et al., 2004).

A series of field campaigns have been conducted in the Mexico City Metropolitan Area, such as the MCMA 2002, 2003 and 2006 field campaigns (Molina et al., 2007; Molina et al, 2008). The objectives of these campaigns are to fully characterize and update the emissions, to investigate the underlying chemical processes that are responsible for secondary air pollutant formation and to facilitate the development of cost-effective control strategies. In this paper, we present measurements of HNO_3 and N_2O_5 during the MCMA 2006 campaign using the ID-CIMS technique for its first field deployment. The results provide insights into the production and gas/particle partitioning of HNO_3 in MCMA.

2 Experimental

2.1 ID-CIMS

The ID-CIMS method has been previously described (Fortner et al, 2004), and only details pertinent to this work are provided. Figure 1 shows a schematic diagram of the ID-CIMS that consists of an ion-drift tube, an ion source, and a quadrupole mass spectrometer. Also depicted in Fig. 1 is the HNO_3 calibration device, which consists of a U-shape 2.54 cm outer diameter (OD) and 17.8 cm long glass tube wrapped with a temperature-regulated heating jacket (the dashed line in Fig. 1). The U-tube has two symmetrical compartments divided by a glass grid in the middle, with one housing a 5.0 cm long Teflon permeation tube (VICI Metronics Inc.) and the other filled with 0.5 cm diameter glass beads to heat the carrier gas uniformly. A corona discharge is used to produce the ions; it consists of a stainless steel needle biased by about -1200 volts (V_1) and a grounded 0.6 cm OD stainless steel tubing. A dry scroll pump (Varian) with a 500 standard liter per minute (slpm) pumping speed draws the ambient air into the ID-CIMS system. A small portion of the air is introduced into the drift tube region through an orifice of about 0.5 mm. Within the drift tube, the reagent ions are produced and the ion-molecule reaction occurs to ionize the neutral analyte species. The ion-drift tube is pumped by an Edwards E2M30 pump. A 10-ring drift tube sealed inside a heavy wall glass tube guides the reagent ions and controls the ion-molecule reaction time. Each stainless steel ring is 7-mm thick with a 40-mm OD and a 14-mm diameter center hole. The rings are connected in series by three Teflon rods and isolated by 3.2 mm nylon spacers. Contiguous rings are connected by a $1.0\pm5\%$ MΩ resistor. A negative voltage

(V2=−32 V) is typically set to develop an electric field in the drift tube. The reagent and product ions are introduced to the MS system through a pinhole of 400 μm, which is also biased by −3 V (V3). Two high vacuum stages housing the quadrupole and the electron multiplier are pumped by two Varian VT-551 turbo molecular pumps with a Varian DS402 backing pump. During measurements, the dry scroll pump draws a flow of 200 slpm ambient air into the inlet, one liter of which is drawn into the drift tube through the front orifice. A flow of N_2 carrying the reagent ions mixes with the air sample within the drift tube and the ion-molecule reaction proceeds throughout the drift region. The typical pressure inside the drift tube is 2.8 torr. The reagent and the product ions are analyzed by an Extrel 150-QC mass spectrometer controlled by the Merlin 3.0 software (Extrel).

The unique character of the ID-CIMS lies in that it enables quantification of neutral species by controlling the ion-molecule reaction time (Δt),

$$A+R^- \xrightarrow{k} P^-+\text{others} \quad \text{(R12)}$$

where A corresponds to the neutral species to be analyzed and quantified, R represents the reagent ion, k is the reaction rate constant, and P denotes the product ion. Because Reaction 12 is kinetically limited (R≫P), the relationship between the ion signals, the ion-molecule reaction rate coefficient, the initial analyte concentration, and the reaction time Δt is given by:

$$[A]=\frac{[P^-]}{k\Delta t[R^-]} \quad \text{(R13)}$$

where $[P^-]$ and $[R^-]$ correspond to the intensities of product and reagent ions measured by the mass spectrometer, respectively. k can be obtained by laboratory measurements or theoretical calculations (Zhao et al., 2004a; 2004b). Δt is determined by the length of the drift tube and the velocity of the reagent ions, U. While moving along the drift region with the carrier gas at a flow velocity of (U_f), ions are also driven by the controllable electric field to achieve a drift velocity (U_d), which is determined by

$$U_d=\mu E \quad \text{(R14)}$$

where μ is the ionic mobility and E is the electric field intensity. μ can be calculated from the reduced ionic mobility, μ_0,

$$\mu=\mu_0(760/P)(T/273.16) \quad \text{(R15)}$$

where P and T are the pressure and temperature inside the drift tube, respectively. The typical reaction time inside the drift tube is 2.6 ms.

2.2 Ion chemistry

The ion chemistry used to detect HNO_3 is similar to that described by Huey and Lovejoy (1996). The reagent ion, SiF_5^-, is produced in two steps. A flow of about 300 standard cubic centimeters per minute (sccm) N_2 doped with ∼0.1% SF_6 flows through the ion source region, where an electron attaches to the SF_6.

$$SF_6+e^-\rightarrow SF_6^- \quad \text{(R16)}$$

A trace amount of SiF_4 is introduced downstream of the ion source and reacts with SF_6^- through a fluoride transfer reaction to produce SiF_5^-.

$$SF_6^-+SiF_4\rightarrow SiF_5^-+SF_5 \quad \text{(R17)}$$

Typically, the residual SF_6^- is less than 2% of the $^{28}SiF_5^-$ reagent ions signal, which is over a million counts per second (cps). SiF_5^- subsequently reacts with HNO_3 at a rate of $(3.8\pm1)\times10^{-10}$ cm^3 molecule^{-1} s^{-1} (Huey and Lovejoy, 1996) to form the $SiF_5^-\cdot HNO_3$ adduct.

$$SiF_5^-+HNO_3\rightarrow SiF_5^-\cdot HNO_3 \quad \text{(R18)}$$

During the field campaign, the count rates of the reagent ion (corresponding to the isotope peak at m/z 125, $^{30}SiF_5^-$, typically 50 kilo cps) and the product ion, $SiF_5^-\cdot HNO_3$ (m/z=186) are recorded consecutively and the integration time is 50 ms and 9 s, respectively. SiF_5^- can form weak clusters with water (Huey and Lovejoy, 1996), but we observe no water clusters in the mass spectrum. A possible explanation is that this water cluster is weakly bonded so it is readily broken up by the collisions – typically 3 Townsend (Td) – in the drift tube.

N_2O_5 is detected using the I^- reagent ion, which is generated inside the ion source through an electron attachment reaction,

$$CF_3I+e^-\rightarrow I^-+CF_3 \quad \text{(R19)}$$

N_2O_5 subsequently reacts with I^- to produce NO_3^-, with a rate constant of 1.3×10^{-9} cm^3 molecule^{-1}s^{-1} (Huey et al., 1995).

$$I^-+N_2O_5\rightarrow NO_3^-+INO_2, \quad \text{(R20)}$$

I^- also reacts with peroxyacyl nitrates (PAN) to form carboxylate ions (Slusher et al., 2004), but this does not interfere with N_2O_5 measurements.

The reduced ionic mobilities (μ_0) of SiF_5^- and I^- have not been reported in the literature. In this work, we determine their values using theoretical calculations. A detailed description of this methodology is provided in appendix A. The values of μ_0 for SiF_5^- and I^- used are 1.89 and 2.09 cm$^2\times$ V$^{-1}\times$s^{-1}, respectively.

2.3 Instrument calibrations

The ID-CIMS can quantitatively determine the concentration of neutral species using Eq. 13. The accuracy of the calculation is affected by uncertainties associated with several parameters, including the reduced ionic mobility, the ion-molecule reaction rate constants, the transmission efficiencies of the quadrupole mass filter, fragmentation in the ion-molecule reaction, etc. These parameters are invariant under a given experimental temperature, especially when the ion-molecule reaction is collision-limited. Furthermore, their uncertainties can be determined by calibration with gas standards of a known concentration.

The HNO_3 calibration employs a permeation device (component *a* in Fig. 1), which is temperature-controlled at 40°C. About a 400 to 500 sccm N_2 carrier gas is fed into the side filled with glass beads and heated to the same temperature as the entire device before entering the permeation tube. After the permeation device, the concentrated HNO_3/N_2 flow with a concentration of 75 to 94 ppb is injected into a 2.5 cm OD Teflon tube in which it is mixed with a 20 to 150 slpm filtered ambient air. The concentrations of the exiting HNO_3 flow ranges between 0.25 and 2 ppb. Prior to each calibration, the permeation device is maintained at an operational condition for more than 6 h to achieve equilibrium.

Due to the "sticky" nature of HNO_3, it is necessary to verify the effective permeation rate under the normal operation condition to account for any possible wall loss during the preparation of the calibration standards. The procedure to verify the permeation rate is similar to the calibration process, but, instead of introducing the HNO_3 standards into the ID-CIMS for calibration, the HNO_3 standard is introduced to a glass bubbler containing a specific amount of pure water ($R>17\,M\Omega$) for a specific time. All tubing is passivated by the HNO_3 standard for a few hours before the final solution is collected. The HNO_3 solution is analyzed by ion chromatography (DIONEX), which is calibrated by ultra pure sodium nitrate (Sigma-Aldrich) solutions. The measured permeation rate is 109 ± 1.2 ng/min, within 10% of the manufacturer's certified value (116 ng/min).

Figure 2 shows a correlation between the volumetrically determined HNO_3 standard concentration and the calculated concentration using the procedure described in Sect. 2.1. The error bars represent the systematic variation in measurements. The value of the slope in Fig. 2 corresponds to the calibration factor used to quantify the uncertainties introduced from the calculation parameters, i.e., the ion-molecule reaction rate constant, reduced ionic mobility, quadrupole transmission efficiency, etc. A calibration factor of 2.2 ± 0.2 is obtained from five independent calibrations at 25°C.

N_2O_5 calibration is conducted with laboratory synthesized samples (Huey et al., 1995). N_2O_5 is formed through two sequential Reactions 9 and 10. O_3 and NO_2 are mixed in a sealed glass reactor and the produced N_2O_5 is collected in a cryotrap (−78.5°C) as white crystal. The first

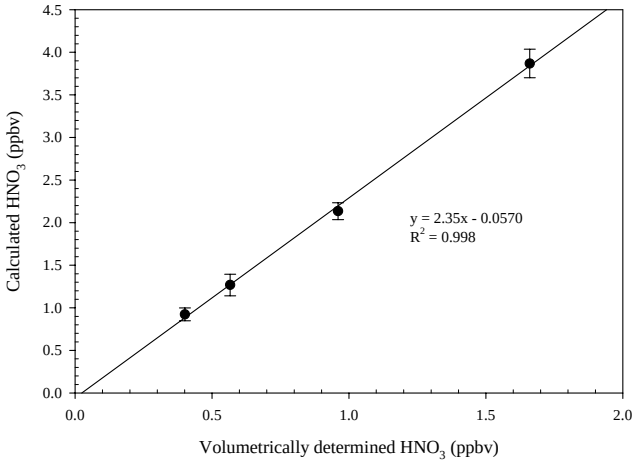

Fig. 2. Plot of calculated versus volumetrically prepared HNO_3 concentrations. The slope corresponds to the calibration factor.

s

batch of N_2O_5 is discarded to remove the water residue inside the cryotrap to minimize HNO_3 formation. During calibration, pure N_2O_5 is kept in an octanol/dry ice bath (−57°C). A small amount of dry N_2 flows through the container and carries N_2O_5 vapor into a 10-cm long absorption cell inside a UV/VIS spectrometer (Perkin Elmer), where the absolute concentration of N_2O_5 is measured by its absorption at 215 nm (σ=2.95×10^{-18} cm^2 $molecule^{-1}$, JPL 2006). Because HNO_3 has a weak absorption at 215 nm (σ=$3.66\times10^{-19}$$cm^2$ $molecule^{-1}$, JPL 2006), the impurity of HNO_3 inside the N_2O_5 reservoir is further quantitated with the ID-CIMS. The results indicate the HNO_3 concentration is less than 5% of the N_2O_5 concentration. Thus, the HNO_3 interference is small for the N_2O_5 absolute calibration. The concentrated N_2O_5 flow is diluted into a 140 slpm flow of N_2 and analyzed by the ID-CIMS. Figure 3 shows N_2O_5 concentrations measured by ID-CIMS against the concentrations determined from UV absorption. The slope in Fig. 3 represents the calibration factor.

During field measurements, HNO_3 background checks are performed once every few hours by directing the ambient air flow through a 5 cm diameter nylon filter. N_2O_5 background signal is checked by passing the ambient air mixed with several hundred ppb of NO through a 31 cm long heated metal tubing. The estimated detection limits of HNO_3 and N_2O_5 are about 38 ppt and 30 ppt for 5-min and 10-s average time, respectively, based on three times the standard deviation of the baseline signals.

2.4 Field setup and characterization of the inlet

The ID-CIMS instrument was deployed at the T0 supersite, located at the Instituto Mexicano del Petróleo (IMP) near the center of the Mexico City Basin (19° 29.400′ N,

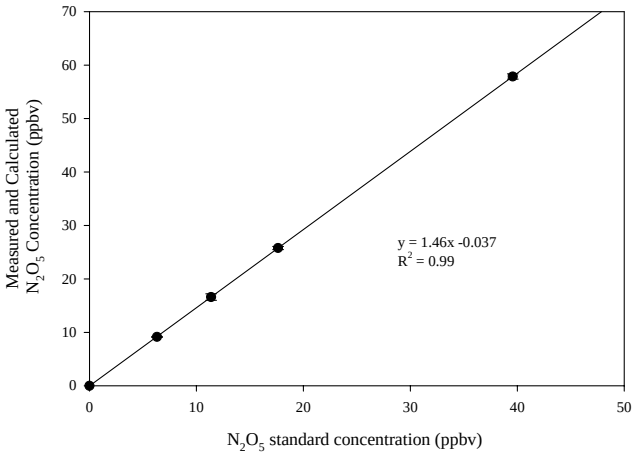

Fig. 3. Plot of measured and calculated N_2O_5 vs. synthesized standards concentration. The slope corresponds to the calibration factor.

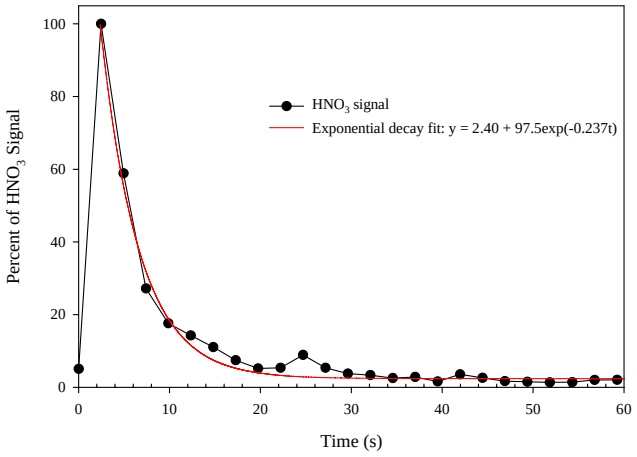

Fig. 4. Spike test of the inlet using a 68 wt% HNO_3 solution exposed to the 12 ft inlet for less than one second. The data were collected at 0.4 Hz.

99° 08.911′ W). The ID-CIMS was housed inside an air-conditioned hut on the roof top of building 32, which was about 30 m above the ground and among a cluster of buildings of similar height. A 2.20-cm ID PFA tubing was used as the inlet, which has been suggested as the best inlet material (Neuman et al., 1999). In order to minimize the surface effects, ambient air was sampled from two feet above the hut ceiling, and the inlet length was about 12 ft to bring the air sample into the ID-CIMS, located a few inches away from the sampling window. From 7 March to 29 March, the average ambient relative humidity (RH) was 41% and the maximum and the minimum temperatures were 30 and 9°C, respectively. There was no precipitation during most days of the campaign except from 24 to 29 March there were several nighttime and afternoon showers. Because HNO_3 gas-aerosol partitioning is sensitive to temperature, the HNO_3 inlet was unheated. Instead, the sampling flow rate was kept at 200 slpm to minimize the sampling residence time (0.42 s) and the entire inlet was kept under ambient conditions. We found that a smaller tubing (0.6 cm) for the inlet reduced the residence time and caused the pressure inside the drift tube to drop considerably, leading to a much shorter ion-molecule reaction time and lower sensitivity.

In order to characterize the performance of the inlet, several tests were conducted by exposing the inlet to elevated HNO_3 (performed at 760 torr, 25°C, and RH=50%). The front of the inlet was exposed to a solution of 68 wt% HNO_3 for less than one second and the ID-CIMS was set to collect data at 0.4 Hz. As shown in Fig. 4, a spike of about 40 ppb HNO_3 was detected by the ID-CIMS within 3 s and the HNO_3 signal decreased by about 80% after 9 s. The decay in the HNO_3 signal was fitted by an exponential decay function ($[HNO_3]$=2.4+97.5 exp(−0.237t)). This implies that the memory effect between adjacent data points was less than 20% if data were averaged every 9 s. However, background checks during the field campaign showed that it usually took nearly two minutes to zero the signal when the nylon filter was installed in the front of the inlet. Therefore, we report the data in 5-min average to eliminate the memory effect.

The inlet for N_2O_5 measurements was made from 2.2-cm ID Teflon tubing. Because we found that N_2O_5 could be permanently lost on the inlet surface due to Reaction 11 during laboratory tests, its length was limited to 2 ft.

2.5 Other instrumentation at T0

An Aerodyne High-Resolution Time-of-Flight Aerosol Mass Spectrometer (HR-ToF-AMS) was used to measure the chemical composition of submicron non-refractory aerosols. This version of the AMS was capable of analyzing organic species and most nitrate and sulfate compounds of different elemental compositions at the same nominal m/z. More details about the AMS are given by DeCarlo et al. (2006) and Canagaratna et al. (2007). Aerosol nitrate concentrations are reported at local temperature and pressure, and should be multiplied by approx. 1.42 to obtain concentrations under standard conditions (STP, 1 atm and 273 K).

An ICMS was employed to measure both gas and aerosol phase acids at T0. A 0.6 cm ID PFA tubing with a length of about 4 m was used as an inlet. The inlet was set about 0.5 m above the roof to minimize surface effects. About 7 slpm air was pumped through the inlet to minimize the residence time. The line was directly connected to the denuder with a self constructed Teflon fitting. About 2 slpm of the air was aspired through a wet effluent diffusion denuder (WEDD) to sample the gas phase acids. Water was continuously pumped through the denuder at a flow rate of 2 ml/min at counter flow to the air. The air to the aerosol collector (AC) was first passed through an activated charcoal denuder at 4 slpm to remove the gas phase species. The air stream was

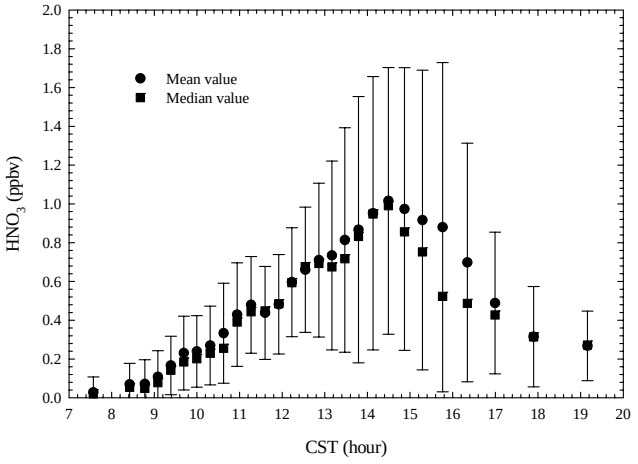

Fig. 5. Averaged HNO_3 diurnal profile during the entire field campaign. Each point is based on 1755 data points and the error bars represent one standard deviation.

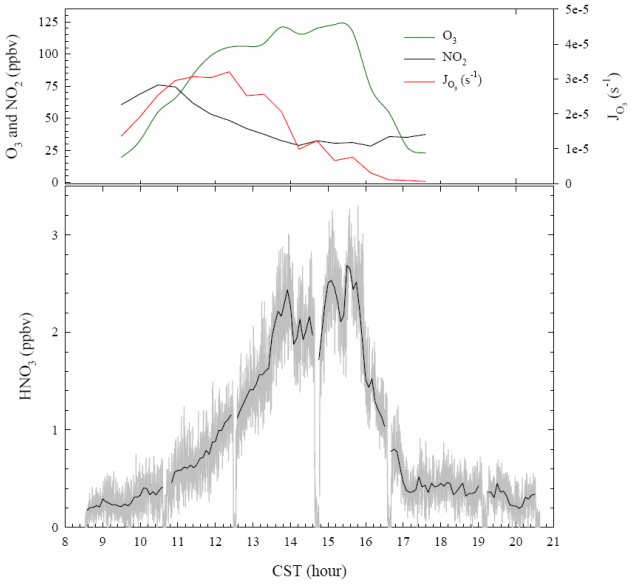

Fig. 6. Time series of HNO_3, O_3, NO_2, and J_{O3} observed on 22 March 2006. Backgrounds of HNO_3 were checked at 08:36, 10:38, 12:30, 14:39, 16:35, 19:20, and 20:35 CST. The solid lines were 5 min average data and the grey area is the 10 s raw data.

mixed with heated water vapor (at 100°C and with a flow rate of 0.6 ml/min), which condensed on aerosol particles. The droplets then impacted on a cooled maze – for details see Fisseha et al. (2006). The gas phase as well as the particle phase extracts were collected each on a concentrator column (TAC-LP1, Dionex) and analyzed alternately using ion chromatography (conductivity detector) with a mass spectrometer in a quasi-continuous mode. The mass spectrometer (MSQ from Dionex) used electro-spray ionization and had a single quadrupole mass detector. The typical detection limit for HNO_3 was 0.06 ppb.

OH radicals were measured at T0 using a laser-induced fluorescence instrument developed at Indiana University. A detailed description of the instrument has been provided by Dusanter et al. (2008). Briefly, it is based on fluorescence assay by gas expansion technique (FAGE) and OH is directly excited and detected at 308 nm. During the MCMA-2006 campaign, the FAGE sample cell was installed on the roof top for inletless sampling. The 30-min average detection limit of FAGE during the campaign ranging from 5×10^5 to 2.6×10^6 molecule/cm^3 of OH.

NO_x and O_3 concentrations used in this work were measured by commercial instruments (Thermo Scientific and Teledyne 400E, respectively), which were regularly calibrated during the campaign. The 5-min average detection limits were 0.1 ppb for both species. The photolysis frequency of O_3 (J_{O_3}) was measured by spectroradiometry, and the technique was described by Volkamer et al. (2007).

3 Results and discussion

3.1 HNO_3 measurements

The measurements of HNO_3 and N_2O_5 were conducted from 7 to 30 March during the MCMA-2006. Due to a power supply failure, no measurements were made from 13 to 17 March. The ID-CIMS was typically configured to measure HNO_3 during daytime and after sunset it was switched to the N_2O_5 measurement mode. All data was collected at 0.1 Hz and presented in Central Standard Time (CST). To minimize the inlet memory effect, all HNO_3 data are reported in a 5-min average and the corresponding detection limit is about 38 ppt, based on three times the standard deviation of the baseline signals.

Figure 5 shows the HNO_3 diurnal profile averaged over the entire campaign. Typically, no significant HNO_3 is observed before 08:00 a.m., and HNO_3 starts to accumulate after 09:00 a.m. and reaches a maximum value of 1 ± 0.65 ppb between 02:00 to 03:00 p.m. After 04:00 p.m., HNO_3 decreases rapidly to less than 0.4 ppb at 06:00 p.m. and gradually approaches 200 ppt, before the ID-CIMS is switched to N_2O_5 measurements. The occurrence of the HNO_3 daily peak is consistent with its photochemical production mechanism; however the magnitude of the HNO_3 peak is lower than that expected for the large NO_x emissions in the MCMA and the strong tropical solar radiation. Another interesting observation is that several hundred ppt HNO_3 is still detected several hours after sunset. Since no significant N_2O_5

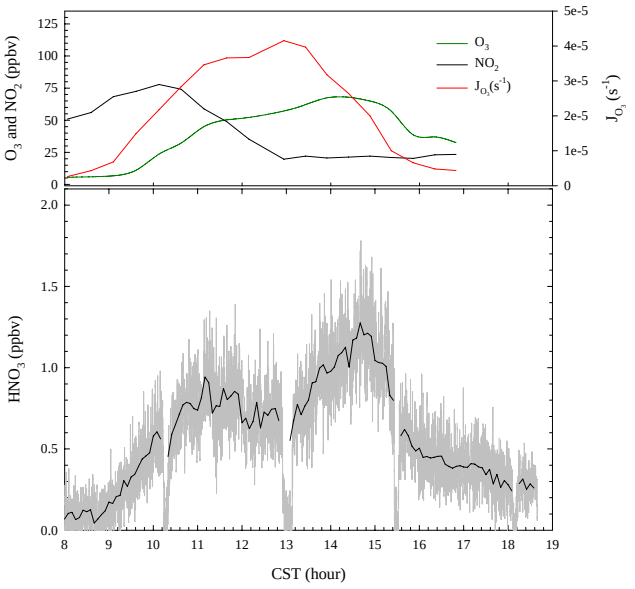

Fig. 7. Time series of HNO_3, O_3, NO_2, and J_{O_3} observed on 23 March 2006. Backgrounds were checked at 08:00, 10:15, 13:00, 15:30, and 18:10 CST. The solid lines were 5 min average data and the grey area is the 10 s raw data.

is present, the nighttime production of HNO_3, i.e. the hydrolysis of N_2O_5 (through Reactions 8 to 11) does not occur.

Figure 6 shows the time series of HNO_3, O_3, NO_2, and J_{O_3} observed on March 22, a sunny but heavily polluted day. From 08:30 a.m. to 10:00 a.m., about 200 ppt HNO_3 is observed and no significant increase occurs before 11:00 a.m., when both NO_2 and J_{O_3} are near their daily maxima. HNO_3 increases steadily after 11:00 a.m. and reaches a value of about 2.4 ppb at 02:00 p.m., while both NO_2 and J_{O_3} are declining. HNO_3 remains at its peak level from 02:00 p.m. to 04:00 p.m., and starts to decrease sharply after 04:00 p.m. due to an air mass change as is evident by a simultaneous sharp decline of ozone. Within one and half hours, only about 400 ppt is observed. The relative diurnal profile and the concentration range measured are similar to that measured in downtown Mexico City by Moya et al. (2004) using FTIR. HNO_3 does not completely disappear even after it is dark, indicating that there are likely other HNO_3 sources present. However, when the ID-CIMS is switched into the N_2O_5 mode, no detectable N_2O_5 is present (<30 ppt). One possible explanation is that the residue HNO_3 is in equilibrium with the ammonium nitrate aerosol, which is also still detectable after sunset.

Figure 7 depicts time series of HNO_3, O_3, NO_2, and J_{O_3} observed on 23 March, a relatively cleaner day than the previous day, as inferred from the higher J_{O_3} value and lower O_3 concentration on 23 March. Before 09:00 a.m., HNO_3 is close to the instrument detection limit. Shortly after 09:00 a.m. HNO_3 increases steadily to about 0.9 ppb at 11:30 a.m. and then starts to decrease to 600 ppt at 01:00 p.m., when OH production is expected to be high. Shortly after 01:00 p.m. HNO_3 starts to increase again and reaches a daily maximum of 1.25 ppb. Afterwards, HNO_3 decreases steadily to 400 ppt at 04:00 p.m. Similar to the previous day, a value of near 300 ppt HNO_3 is still observable at about 06:30 p.m. When the ID-CIMS is switched into the N_2O_5 mode, no detectable N_2O_5 is present. Note that 22 and 23 March represent the typical "more polluted" and "cleaner" conditions encountered during the field campaign, respectively.

O_3 in Figs. 6 and 7 exhibits a similar profile as HNO_3 but with a delay in the peak time compared with J_{O_3}. This is expected as both compounds are produced from two competitive reactions in the photooxidation process according to Reactions 1, 21 and 22.

$$\mathrm{VOC+OH} \xrightarrow{\mathrm{O_2}} \mathrm{RO_2} \qquad \text{(R21)}$$

$$\mathrm{RO_2} \xrightarrow{\mathrm{NO,hv}} \mathrm{O_3} \qquad \text{(R22)}$$

As discussed above, although HNO_3 production began immediately after sunrise (~06:30 a.m.), no significant accumulation of HNO_3 is typically observed before 09:00 a.m. Thus, it is evident that the gas-phase chemistry alone cannot explain the observations in the HNO_3 diurnal profiles, i.e., the slow rise after sunrise and the residual HNO_3 after sunset. Heterogeneous processing of HNO_3 in the particle-phase needs to be accounted for to explain the HNO_3 measurements during MCMA 2006. The heterogeneous reaction between HNO_3 and NH_3 in the particle-phase to form ammonium nitrate represents an important process to modulate the gaseous HNO_3 concentration,

$$\mathrm{HNO_3(g)+NH_3(g) \leftrightarrow NH_4NO_3(s)} \qquad \text{(R23)}$$

Depending on the RH, ammonium nitrate formed in Reaction 23 exists as a solid or an aqueous solution of NH_4^+ and NO_3^-. The equilibrium constant, K_p, depends on the temperature (Seinfeld and Pandis, 1998),

$$\ln K_p = 84.6 - (24220/T) - 6.1 \times \ln(T/298) \qquad \text{(R24)}$$

For the measurements relevant to MCMA 2006, the RH is fairly low (<41% averaged over the campaign period). The dry environment at the MCMA prevents NH_4NO_3 from deliquescence and NH_4NO_3 is expected to be a solid. High ammonia (NH_3) concentrations (>35 ppb in the early morning) were reported during the MCMA 2003 campaign (Moya et al., 2004). Although no direct measurements of NH_3 are available at T0 during MCMA 2006, NH_3 measured at the T1 site (~30 km to the northeast of T0) using a quantum-cascade laser (QCL) spectrometer (Fischer and Littlejohn, 2007) shows an average concentration of 26.7±13.7 ppb from 21 to 31 March.

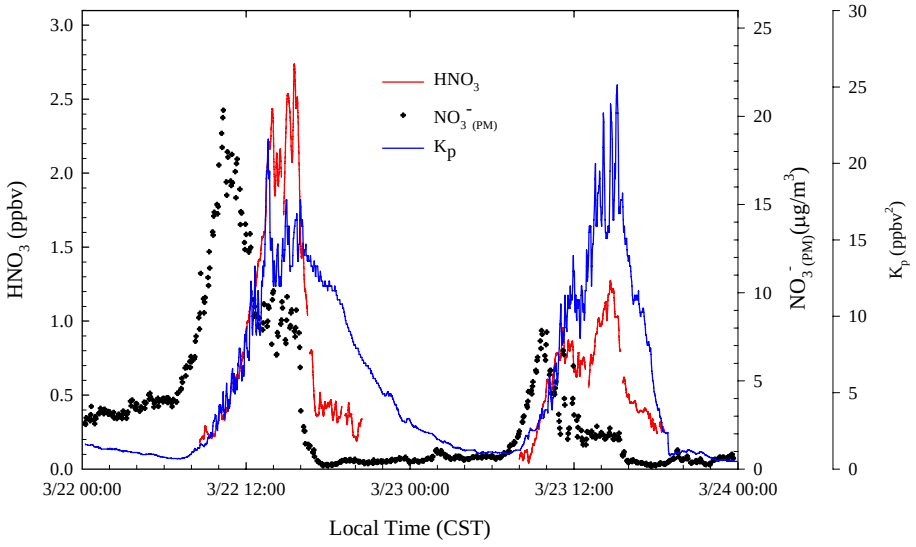

Fig. 8. Gaseous HNO_3, submicron aerosol nitrate ($NO^-_{3(PM)}$) ($1\,\mu g/m^3$ nitrate under ambient pressure and temperature can contribute to 0.51 ppb gaseous HNO_3 after complete evaporation), and the calculated dissociation constant K_p of Reaction 26 for 22 and 23 March 2006.

Figure 8 shows a comparison between gaseous HNO_3 and submicron aerosol nitrate ($NO^-_{3(PM)}$) mass concentration measured by the AMS on 22 and 23 March. The calculated equilibrium constant (K_p) of Reaction 23 is also plotted in Fig. 8, which is a function of ambient temperature. There are several prominent features in Fig. 8. The aerosol nitrate starts to increase right after sunrise and reaches a maximum in the early morning. The aerosol nitrate peak occurs several hours earlier than that of the gaseous HNO_3 concentration. The aerosol nitrate drops sharply after the morning peak and remains low throughout the afternoon and night hours. The measured HNO_3 concentration and the calculated K_p are anti-correlated with $NO^-_{3(PM)}$. On the other hand, there appears to exist a good correlation between the measured HNO_3 concentration and calculated K_p: both slowly increase at the morning hours and their peaks coincide. Hence, the slow rise in the measured HNO_3 concentration is likely explained by gas/aerosol partitioning. HNO_3 photochemically produced from Reaction 1 is scavenged from the gas phase by the particle-phase reaction with NH_3 to form aerosol nitrate, when ambient temperature is low but ammonia is high (Moya et al., 2004) and aerosol nitrate is favorable (K_p<6). The gas/aerosol partitioning hence likely accounts for the delayed rise and daily maximum of measured HNO_3 compared to those of measured aerosol nitrate. As the temperature rises and the NH_3 concentration likely decreases strongly (Moya et al., 2004) during the course of the day, the equilibrium favors gaseous HNO_3. HNO_3 is released back to the gas-phase from the evaporation of aerosol nitrate, leading to a peak in the gas-phase concentration even when its photochemical production decreases. After sunset, the HNO_3 photochemical production ceases, as reflected in the decrease of measured HNO_3, but a few hundreds of ppt HNO_3 are still measured. Evidently, a small increase of submicron aerosol nitrate is observed from 06:00 p.m. to about 07:30 p.m. on 22 and 23 March, while HNO_3 is decreasing. At the same time, the ambient temperature is also decreasing, in favor of the conversion of gaseous HNO_3 into aerosol nitrate. Therefore, the lingering nighttime HNO_3 likely originates from the residue ammonium nitrate aerosol, instead of the hydrolysis of N_2O_5.

It should be pointed out that the above discussions are based on surface measurements only. However, higher concentrations of NO_3 and N_2O_5 above the nocturnal surface layer (and thus away from direct NO emissions) have been reported in other field studies (Brown et al., 2007; Geyer and Stutz, 2004; Stutz et al, 2004). Thus, some of the nighttime HNO_3 can also be formed aloft and then transported down to the surface. Figure 8 also shows that on a daily basis a higher aerosol nitrate corresponds to a higher HNO_3 peak, when the difference in K_p is insignificant. This probably explains the difference in the measurements of $NO^-_{3(PM)}$ and HNO_3 between 22 and 23 March 2006. Figure 9 shows additional daily profiles of $NO^-_{3(PM)}$ and HNO_3 observed on 11 and 12 March, showing a similar correlation between $NO^-_{3(PM)}$ and HNO_3. As discussed before, HNO_3 is present primarily in the aerosol phase during the early morning hours due to lower temperatures and higher NH_3. HNO_3 is released from $NO^-_{3(PM)}$ as the ambient air temperature rises and reaches the daily maximum around 02:00 p.m. After sunset both $NO^-_{3(PM)}$ and HNO_3 decrease, but remain in detectable amounts. Therefore, we conclude that during MCMA 2006 at T0 the gas/particle partitioning plays a key role in regulating gaseous HNO_3 and is essential to account for the measurements of gaseous HNO_3 and aerosol nitrate.

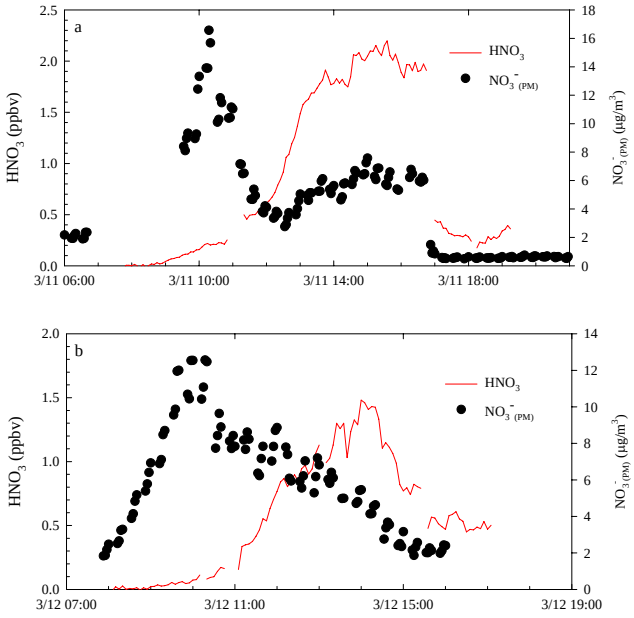

Fig. 9. Gaseous HNO_3, submicron aerosol nitrate ($NO^-_{3(PM)}$) observed on 11 **(a)** and 12 March **(b)**.

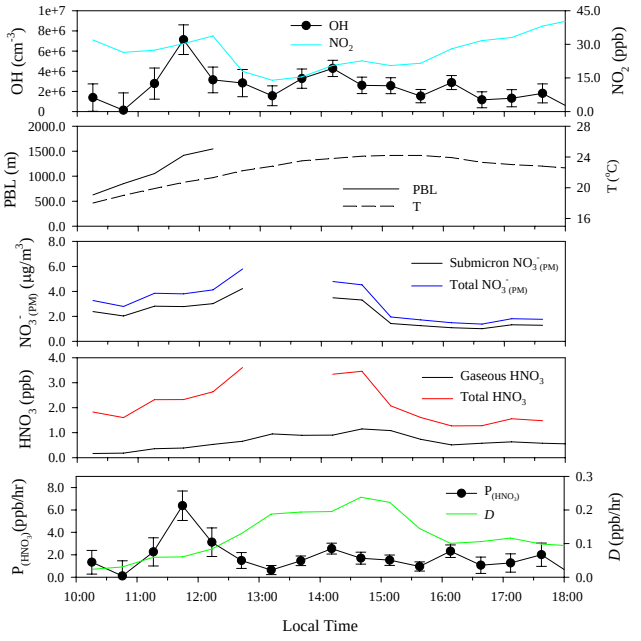

Fig. 10. 30 min average OH, NO_2, temperature, PBL, aerosol nitrate ($NO^-_{3(PM)}$), gaseous HNO_3 and total HNO_3 (assuming all $NO^-_{3(PM)}$ is in gas-phase), calculated HNO_3 production rate (P_{HNO_3}), and gaseous HNO_3 dry deposition rate on 20 March at T0.

Our results are consistent with earlier studies conducted in MCMA. Salcedo et al. (2006) measured aerosol nitrate during the MCMA 2003 campaign. They found that the morning particulate nitrate increased in a manner consistent with the production of nitric acid, but after 11:00 a.m. the aerosol nitrate decreased while HNO_3 production continued. This observation was explained by the increase of the planetary boundary layer (PBL) height and temperature and the decrease in the RH and NH_3 as the day progressed. Also, it has been suggested that gas-particle partitioning plays a dominant role in the fate of aerosol ammonium nitrate over larger spatial scales (DeCarlo et al., 2008).

In order to assess the HNO_3 budget at T0 during MCMA 2006, we calculate the HNO_3 production rate (P_{HNO_3}) from Reaction 1 between 10:00 a.m. and 06:00 p.m. on 20 March with a rate constant recommended by Okumura and Sander (2005). The results, along with OH, NO_2, HNO_3, $NO^-_{3(PM)}$, PBL height, and temperature measurements, are shown in Fig. 10. From 10:15 a.m. to 11:45 a.m., P_{HNO_3} increases from near 1 ppb/hr to about 6.4 ppb/hr, while total HNO_3 (HNO_3+submicron $NO^-_{3(PM)}$) only increases moderately. This can be partially explained by the significant increase in PBL, by a factor of about 2.5. After 11:45 a.m., P_{HNO_3} decreases to about 1.7 ppb/hr at about 12:45 p.m., which is mainly caused by the decreases of both OH and NO_2, and fluctuates near 1.7 ppb/hr thereafter. Total HNO_3 peaks around early afternoon and starts decreasing after 02:30 p.m.. From the HNO_3 data, we estimate a maximum total HNO_3 of about 3 ppb, which is significantly less than expected from the calculated P_{HNO_3}. Thus processes such as dry deposition and reactions on dust must play a role to remove HNO_3 from the ambient air in the MCMA. Heterogeneous reaction of HNO_3 on dust surfaces has been shown to be important during MILAGRO, leading to permanent removal of HNO_3 to form non-volatile mineral nitrates such as $Ca(NO_3)_2$ (Querol et al., 2008; Fountoukis et al., 2007; Hodzic et al., 2007). This nitrate can exist in the supermicron size range and thus is not measured by the AMS. Querol et al. (2008) estimated nitrate content in the $PM_{10}-PM_{2.5}$ range accounts for ∼20% of the total nitrate at T0, with a higher fraction in the early part of MILAGRO due to reduced precipitation and increased dust concentration. Since the AMS measures PM_1 aerosols, there will be some additional nitrate associated with dust in the $PM_{2.5}-PM_1$ range beyond that quantified by Querol et al. If the dust size distribution in Mexico is similar to that reported by Maring et al. (2003) and the dust reactivity is uniform across the dust size distribution, this size range will likely account for about ∼1/3 additional dust nitrate beyond that $PM_{10}-PM_{2.5}$ size range, i.e. ∼7% of the total aerosol nitrate, such that the total nitrate can be estimated as 1.37 times the submicron nitrate. From 10:15 a.m. to 12:45 a.m., the observed increase of total HNO_3 is about 1.8 ppb and 1.3 ppb of which is due to aerosol nitrate, while the total HNO_3 produced from Reaction 1 is about 2.6 ppb after applying the dilution factor of 2.5. Therefore, aerosol phase nitrate and gaseous HNO_3 can account for about 50% and 19% of the HNO_3 produced from Reaction 1, respectively.

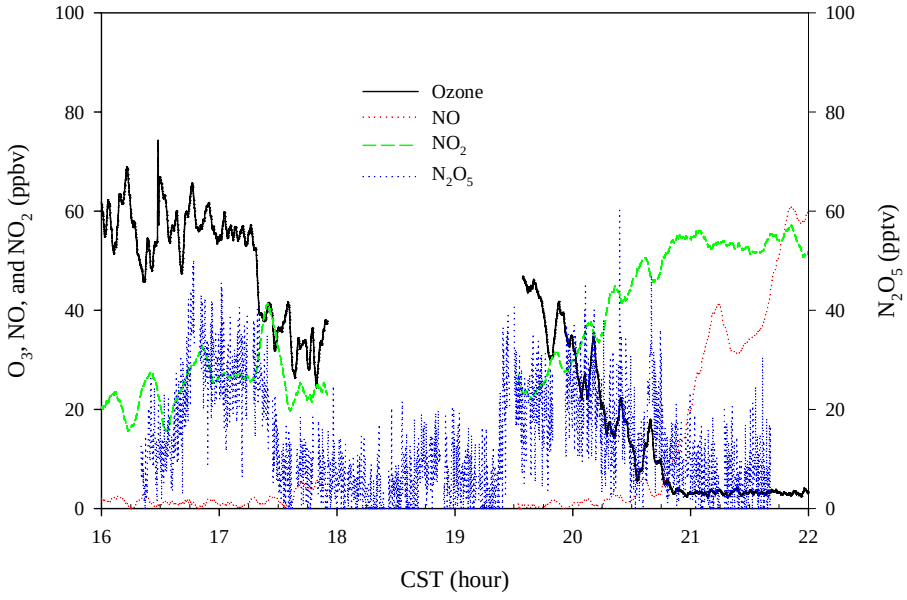

Fig. 11. N_2O_5 measured on 26 March. Also shown are plots of NO, NO_2, and O_3. The gap in the measurements was due to instrument calibrations.

Finally we evaluate the potential effect of dry deposition on the measured HNO_3 concentrations. The dry deposition (D) can be estimated as:

$$D = v_d * C \quad \text{(R25)}$$

where v_d is the deposition velocity and C is the concentration. v_d is much larger for HNO_3 than aerosol nitrate (e.g. Kajino et al., 2008), and to first approximation we estimate the deposition flux by only estimating that of nitric acid. HNO_3 deposition velocity is calculated according to the method described by Fast et al. (2006) and an average value of about 5 cm s^{-1} is obtained from 10:15 to 12:45 a.m., which is consistent with the literature values (Myles et al., 2007; Pryor and Klemm, 2004). Based on the observed PBL height and gaseous HNO_3, the estimated dry deposition rate (also shown in Fig. 10) would reduce HNO_3 concentrations over the depth of the boundary layer by $\sim$0.08 ppb hr^{-1}, which accounts for additional 8% of the total HNO_3 production. Although there is still 23% of the HNO_3 production cannot be accounted for, it is well within the experimental uncertainties of all the parameters used in the estimation. Figure 10 also shows that temperature affects the partitioning between $NO_{3(PM)}^-$ and HNO_3. Temperature increases gradually from 18°C to 24°C from 10:00 a.m. to 03:00 p.m. and decreases slightly thereafter. HNO_3 clearly follows a similar trend as temperature; however, $NO_{3(PM)}^-$ shows an opposite trend with higher concentrations in the morning than in the afternoon.

3.2 N_2O_5 Measurements

The ID-CIMS instrument is typically switched to measure N_2O_5 after sunset during the MCMA-2006 campaign. Nighttime N_2O_5 is typically below the detection limit of the instrument. Because NO concentration frequently exceeds 100 ppb after 07:00 p.m. and O_3 is rapidly depleted by freshly emitted NO, Reactions 9 and 10 are inhibited at the surface level. Therefore, NO_3 and N_2O_5 do not play a major role during the nighttime chemistry at the surface, although it is likely that some HNO_3 may be formed above the PBL where the N_2O_5 chemistry is still occurring at night and mixes downward (Stutz et al., 2004). However, as an exception, two N_2O_5 peaks are observed in the late afternoon and early evening on 26 March (Fig. 11). There was a scattered shower starting in the early afternoon and no HNO_3 was observed thereafter. At 04:00 p.m., the rain stopped and the sky remained cloudy. The concentrations of O_3 and NO_2 are about 60 ppb and 20 ppb, respectively, while the NO concentration is less than 2 ppb. The ID-CIMS was switched to the N_2O_5 mode at 04:20 p.m. and the measurement continued until 09:40 p.m., when NO and NO_2 were about 40 ppb and 60 ppb but O_3 was only 3 ppb. Background checks were performed at the beginning and at the end of the measurement. Two N_2O_5 peaks near 40 ppt are observed around 05:00 p.m. and 08:00 p.m., when both NO_2 and O_3 are still substantial, but no fresh NO emission is present. From 05:45 p.m. to 07:20 p.m., the T0 site was hit by another intermittent shower; no N_2O_5 was observed and the NO_x and O_3 instruments were off-line for calibrations. After 07:30 p.m., O_3 is negatively correlated with NO_2 due to Reaction 8. About 08:50 p.m., NO starts to

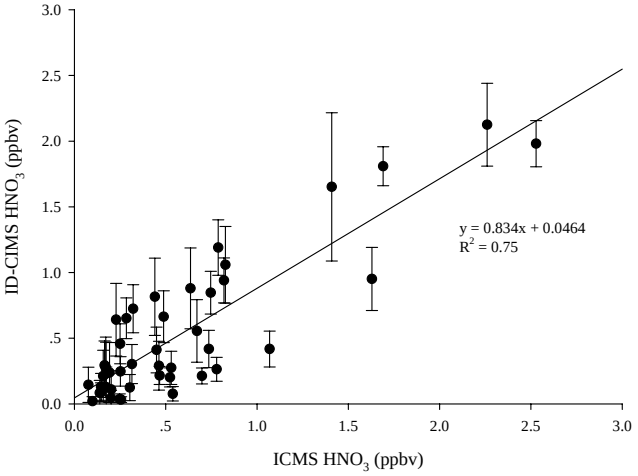

Fig. 12. Inter-comparison between the ID-CIMS and ICMS based on 45 overlapping data points collected from 8 to 29 March 2006.

increase significantly and nearly all O_3 is depleted, as N_2O_5 disappears. The temperature during the observation period is relatively low (average 14.6°C). Since the ID-CIMS responds to both NO_3 and N_2O_5 by detecting the same nitrate anion at m/z 62, we estimate a steady state NO_3 concentration based on Reactions 9 and 10, assuming that the ID-CIMS responds to NO_3 and N_2O_5 equivalently:

$$k_9[O_3][NO_2]+k_{-10}[N_2O_5]=k_{10}[NO_2][NO_3] \quad \text{(R26)}$$

$$[NO_3^-]=[N_2O_5]+[NO_3] \quad \text{(R27)}$$

where $[NO_3^-]$, k_9, k_{10}, and k_{-10} are the total NO_3^- signal observed by the ID-CIMS, the rate constant of Reaction 9, the forward reaction rate constant of Reaction 10, and the reverse reaction rate constant of Reaction 10, respectively. k_9, k_{10}, and k_{-10} are calculated according to formulas recommended by JPL (2006). The results suggest that NO_3 radical account for less than 4% of the total signal.

3.3 Inter-comparison with ICMS

An ICMS instrument is set up side-by-side with the ID-CIMS during the MCMA-2006 field campaign. The ICMS utilizes a denuder to selectively collect gas phase HNO_3 into aqueous solutions, which are then analyzed by an electrospray mass spectrometer. Since the ICMS produce one data point about every two hours, its time series does not match with the temporal resolution of about 10 s from the ID-CIMS measurements. We compare the results between the two instruments for periods when both instruments are collecting data and the ID-CIMS data are averaged to represent the data during a similar period. The results are plotted in Fig. 12, showing a good correlation (R^2=0.75) between the two techniques. We also perform a t-test for these two sets of data and a significance value of 0.68 further confirms that statistically the results from the two techniques are in good agreement. The ID-CIMS data are about 17% lower than the ICMS data, and the y-intercept is much smaller than the detection limit of either instrument. However, because the overlapping data points are rather scarce, the positive trend at low values is not as good as at the higher values. One possible explanation is that the variations of HNO_3 (indicated by the error bars) affect the correlation more significantly at low concentrations than at high concentrations. Also, the error bars can account for the difference in response time between the two instruments, i.e. a higher level of variation indicates faster changing of HNO_3, which is easily captured by the ID-CIMS.

4 Conclusions

An ID-CIMS instrument was deployed during the MCMA-2006 campaign to measure HNO_3 and N_2O_5 at the T0 urban site. The objective of this work is to characterize the NO_x chemistry and budget in the MCMA. Diurnally, HNO_3 is less than 200 ppt during the night and in the early morning, increases steadily from around 09:00 a.m. CST, reaches a peak value of 0.5 to 3 ppb in the early afternoon, and then declines sharply to less than half of the peak value near 05:00 p.m. CST. The HNO_3 mixing ratio is found to negatively correlate with submicron aerosol nitrate, suggesting that the gaseous HNO_3 concentration is primarily produced by the photochemistry and regulated by the gas-particle partitioning process. Gaseous HNO_3 and submicron aerosol nitrate can account for 19% and 36% of the calculated HNO_3 production rate based on OH and NO_2 observations. Dry deposition can only explain about 8% of the total HNO_3 production. However, additional losses by HNO_3 reaction on dust particles likely contribute to about another 14% of the total HNO_3 production. Thus, only 23% of the HNO_3 production cannot be accounted for but it is well within the experimental uncertainties. Inter-comparison between the ID-CIMS and the ICMS shows a good agreement (R^2=0.75) in the HNO_3 measurements. During most times of the MCMA-2006 campaign, N_2O_5 is below the detection limit of the ID-CIMS due to high NO mixing ratio at the surface, except on one occasion on 26 March when transient N_2O_5 peaks of 40 ppt are detected under cloudy conditions. At the surface, N_2O_5 appears to play a minor role in HNO_3 production, but it still can exist in significant concentration in the upper boundary layer and undergoes heterogeneous reactions to form HNO_3, which can be transported to the surface.

Appendix A

The reduced ionic mobilities, μ_0, of SiF_5^- and I^- are not reported in the literature. In this work, we determine their values according to Mason and McDaniel (1988),

$$\mu_0 = \frac{1.85\times10^4}{\bar{\bar{\Omega}}\sqrt{T_{\rm eff}}}\left(\frac{m+M}{mM}\right)^{1/2}\,{\rm cm}^2\times V^{-1}\times{\rm s}^{-1}, \quad \text{(A1)}$$

where $T_{\rm eff}$ is the effective temperature of the carrier gas (in K), m and M are the masses (in atomic mass units) of the ion (SiF_5^- or I^-) and the carrier gas (N_2), respectively, and $\bar{\bar{\Omega}}$ is the momentum-transfer collision integral (in cm^2). $T_{\rm eff}$ is given by

$$\frac{3}{2}k_bT_{\rm eff} = \frac{3}{2}k_b\,T + \frac{1}{2}mU_f^2 \quad \text{(A2)}$$

where k_b is Boltzmann's constant and T is the temperature of the carrier gas. $\bar{\bar{\Omega}}$ is obtained from the tabulated values (Viehland et al., 1975) based on ion-neutral interaction potentials. Because no experimental data are available to characterize the ion-neutral interactions in the SiF_5^-/N_2 or I^-/N_2 system, we perform ab initio calculations to obtain the ion-neutral interaction potentials using the Gaussian 03 software package on an SGI Origin 3800 supercomputer (Lei et al., 2000; Suh et al., 2002; Zhang et al., 2002; Suh et al., 2003). The geometry optimization and energy calculations at a series of center-to-center distances for SiF_5^-/N_2 and I^-/N_2 systems are conducted using density function method B3LYP/6-31G(d,p) and B3LYP/LANL2DZ, respectively. The results are then fitted with a potential model (Viehland et al., 1975)

$$V(r) = \frac{B}{r^{12}} - \frac{C_6}{r^6} - \frac{C_4}{r^4} \quad \text{(A3)}$$

where the B term represents the short-range repulsion energy, C_6 denotes the charge-induced quadrupole attraction plus the London dispersion attraction, and C_4 represents the attraction between the ion and the dipole induced in N_2. Based on the calculated potential well depth, ε, and the minimum position, r_m, the corresponding value of $\bar{\bar{\Omega}}$ is obtained. Table A1 provides a summary of the calculations. The predicted values of μ_0 for SiF_5^- and I^- are 1.89 and $2.09\,{\rm cm}^2\times{\rm V}^{-1}\times{\rm s}^{-1}$, respectively.

Table A1. Ion-neutral potentials of SiF_5^-/N_2 and I^-/N_2 systems based on *ab initio* calculations

	SiF_5^-/N_2	I^-/N_2
ε (eV)	0.050	0.057
r_m(A)	4.82	4.06
B (eV·A^{12})	8.62×10^6	5.29×10^5
C_6 (eV·A^6)	824.96	220.38
C_4 (eV·A^4)	20.98	8.39
$\bar{\bar{\Omega}}(10^{-16}\,{\rm cm}^2)$	73.16	51.83

Acknowledgements. This research was funded by the Center for Atmospheric Chemistry and Environment at the Texas A&M University and by the Robert A. Welch Foundation (Grant A-1417). Additional support was provided by the Texas A&M University Supercomputing Facilities. The authors are grateful to Nancy A. Marley and Jeffrey S. Gaffney for providing the temperature and RH data, Jerome D. Fast for providing calculated HNO_3 dry deposition rates, William E. Eichinger for providing boundary height data at T0, and Marc L. Fischer for providing NH_3 data at T1 site. A. C. A. and J. L. J. acknowledged support from NSF (ATM-0449815 and ATM-0528634), DOE (BER, ASP program, DE-FG02-05ER63981), and a NASA Graduate Fellowship to ACA (NNG04GR06H), K. G. and J. D. acknowledged support from SNSF and INTROP (1024, 1034), and L. T. M. acknowledged support from NSF (ATM-0528227).

Edited by: S. Madronich

References

Anlauf, K. G., Mactavish, D. C., Wiebe, H. A., Schiff, H. I., and Mackay, G. I.: Measurement of atmospheric nitric-acid by the filter method and comparisons with the tunable diode-laser and other methods, Atmos. Environ., 22, 1579–1586, 1988.

Brown, S. S., Stark, H., Ciciora, S. J., and Ravishankara, A. R.: In-situ measurement of atmospheric NO_3 and N_2O_5 via cavity ring-down spectroscopy, Geophys. Res. Lett., 28, 3227–3230, 2001.

Brown, S. S., Stark, H., Ciciora, S. J., McLaughlin, R. J., and Ravishankara, A. R.: Simultaneous in situ detection of atmospheric NO_3 and N_2O_5 via cavity ring-down spectroscopy, Rev. Sci. Instrum., 73, 3291–3301, 2002.

Brown, S. S., Ryerson, T. B., Wollny, A. G., Brock, C. A., Peltier, R., Sullivan, A. P., Weber, R. J., Dube, W. P., Trainer, M., Meagher, J. F., Fehsenfeld, F. C., and Ravishankara, A. R.: Variability in nocturnal nitrogen oxide processing and its role in regional air quality, Science, 311, 67–70, 2006.

Brown, S. S., Dube, W. P., Osthoff, H. D., Stutz, J., Ryerson, T. B., Wollny, A. G., Brock, C. A., Warneke, C., De Gouw, J. A., Atlas, E., Neuman, J. A., Holloway, J. S., Lerner, B. M., Williams, E. J., Kuster, W. C., Goldan, P. D., Angevine, W. M., Trainer, M., Fehsenfeld, F. C., and Ravishankara, A. R.: Vertical profiles in NO_3 and N_2O_5 measured from an aircraft: Results from the NOAA P-3 and surface platforms during the new England air quality study 2004, J. Geophys. Res.-Atmos., 112, D22304, doi:10.1029/2007JD008883, 2007.

CAM (Comisión Ambiental Metropolitana): Inventario de emisiones 2004 de la Zona Metropolitana del Valle de México, Secretaría del Medio Ambiente, Gobierno de México, México, online available at: http://www.sma.df.gob.mx/, 2006.

Canagaratna, M. R., Jayne, J. T., Jimenez, J. L., Allan, J. D., Alfarra, M. R, Zhang, Q., Onasch, T. B., Drewnick, F., Coe, H., Middlebrook, A., Delia, A., Williams, L. R., Trimborn, A. M., Northway, M. J., DeCarlo, P. F., Kolb, C. E., Davidovits, P., and Worsnop, D. R.: Chemical and Microphysical Characterization of Ambient Aerosols with the Aerodyne Aerosol Mass Spectrometer, Mass Spectrom. Revi., 26, 185–222, 2007.

DeCarlo, P. F., Kimmel, J. R., Trimborn, A., Northway, M. J., Jayne, J. T., Aiken, A. C., Gonin, M., Fuhrer, K., Horvath, T., Docherty, K. S., Worsnop, D. R., and Jimenez, J. L.: Field-deployable, high-resolution, time-of-flight aerosol mass spectrometer, Anal. Chem., 78, 8281–8289, 2006.

DeCarlo, P. F., Dunlea, E. J., Kimmel, J. R., Aiken, A. C., Sueper, D., Crounse, J., Wennberg, P. O., Emmons, L., Shinozuka, Y., Clarke, A., Zhou, J., Tomlinson, J., Collins, D. R., Knapp, D., Weinheimer, A. J., Montzka, D. D., Campos, T., and Jimenez, J. L.: Fast airborne aerosol size and chemistry measurements above Mexico City and Central Mexico during the MILAGRO campaign, Atmos. Chem. Phys., 8, 4027–4048, 2008, http://www.atmos-chem-phys.net/8/4027/2008/.

Dusanter, S., Vimal, D., Stevens, P. S., Volkamer, R., and Molina, L. T.: Measurements of OH and HO2 concentrations during the MCMA-2006 field campaign – Part 1: Deployment of the Indiana University laser-induced fluorescence instrument, Atmos. Chem. Phys. Discuss., 8, 13 689–13 739, 2008, http://www.atmos-chem-phys-discuss.net/8/13689/2008/.

Fast, J. D., Gustafson, W. I., Easter, R. C., Zaveri, R. A., Barnard, J. C., Chapman, E. G., Grell, G. A., and Peckham, S. E.: Evolution of ozone, particulates, and aerosol direct radiative forcing in the vicinity of Houston using a fully coupled meteorology-chemistry-aerosol model, J. Geophys. Res.-Atmos., 111, D21305, doi:10.1029/2005jd006721, 2006.

Finlayson-Pitts, B. J., and Pitts, J. N.: Chemistry of the upper and lower atmosphere: Theory, experiments and applications, Academic Press, San Diego, CA, USA, xxii, 969 pp., 1999.

Fischer, M. L. and Littlejohn D.: Ammonia at Blodgett Forest, Sierra Nevada, USA, Atmos. Chem. Phys. Discuss., 7, 14 139–14 169, 2007, http://www.atmos-chem-phys-discuss.net/7/14139/2007/.

Fisseha, R., Dommen, J., Gaeggeler, K., Weingartner, E., Samburova, V., Kalberer, M., and Baltensperger, U.: Online gas and aerosol measurement of water soluble carboxylic acids in zurich, J. Geophys. Res.-Atmos., 111, D12316, doi:10.1029/2005JD006782, 2006.

Fortner, E. C., Zhao, J., and Zhang, R. Y.: Development of ion drift-chemical ionization mass spectrometry, Anal. Chem., 76, 5436–5440, 2004.

Fountoukis, C., Nenes, A., Sullivan, A., Weber, R., VanReken, T., Fischer, M., Matías, E., Moya, M., Farmer, D., and Cohen, R. C.: Thermodynamic characterization of Mexico City aerosol during MILAGRO 2006, Atmos. Chem. Phys. Discuss., 7, 9203–9233, 2007, http://www.atmos-chem-phys-discuss.net/7/9203/2007/.

Furutani, H. and Akimoto, H.: Development and characterization of a fast measurement system for gas-phase nitric acid with a chemical ionization mass spectrometer in the marine boundary layer, J, Geophys. Res.-Atmos., 107, 4016, doi:10.1029/2000JD000269, 2002.

Geyer, A. and Stutz, J.: Vertical profiles of NO_3, N_2O_5, O_3, and NO_x in the nocturnal boundary layer: 2. Model studies on the altitude dependence of composition and chemistry, J. Geophys. Res.-Atmos., 109, D12307, doi:10.1029/2004JD005217, 2004.

Hering, S. V., Lawson, D. R., Allegrini, I., Febo, A., Perrino, C., Possanzini, M., Sickles, J. E., Anlauf, K. G., Wiebe, A., Appel, B. R., John, W., Ondo, J., Wall, S., Braman, R. S., Sutton, R., Cass, G. R., Solomon, P. A., Eatough, D. J., Eatough, N. L., Ellis, E. C., Grosjean, D., Hicks, B. B., Womack, J. D., Horrocks, J., Knapp, K. T., Ellestad, T. G., Paur, R. J., Mitchell, W. J., Pleasant, M., Peake, E., Maclean, A., Pierson, W. R., Brachaczek, W., Schiff, H. I., Mackay, G. I., Spicer, C. W., Stedman, D. H., Winer, A. M., Biermann, H. W., and Tuazon, E. C.: The nitric-acid shootout – field comparison of measurement methods, Atmos. Environ., 22, 1519–1539, 1988.

Hodzic, A, Flocke, F. M., Madronich, S., Fast, J., Zheng, W., Weinheimer, A., Montzka, D., Knapp, D., Mauldin, L., Wennberg, P., Crounse, J. D., McCabe, D., Clarke, A., Hostetler, C. A., and Hair, J. W.: Contribution of dust particles to the heterogeneous removal of acidic gases from the atmosphere during the MIRAGE experiment, Eos Trans. AGU, 88(52), Fall Meet. Suppl., Abstract A23C-1476, 2007.

Horii, C. V., Munger, J. W., Wofsy, S. C., Zahniser, M., Nelson, D., and McManus, J. B.: Atmospheric reactive nitrogen concentration and flux budgets at a Northeastern US forest site, Agr. Forest Meteorol., 136, 159–174, 2006.

Huey, L. G., Hanson, D. R., and Howard, C. J.: Reactions of SF_6^- and I^- with atmospheric trace gases, J. Phys. Chem., 99, 5001–5008, 1995.

Huey, L. G. and Lovejoy, E. R.: Reactions of SiF_5^- with atmospheric trace gases: Ion chemistry for chemical ionization detection of HNO_3 in the troposphere, Int. J. Mass Spectrom., 155, 133–140, 1996.

Huey, L. G., Dunlea, E. J., Lovejoy, E. R., Hanson, D. R., Norton, R. B., Fehsenfeld, F. C., and Howard, C. J.: Fast time response measurements of HNO_3 in air with a chemical ionization mass spectrometer, J. Geophys. Res.-Atmos., 103, 3355–3360, 1998.

Huey, L. G., Tanner, D. J., Slusher, D. L., Dibb, J. E., Arimoto, R., Chen, G., Davis, D., Buhr, M. P., Nowak, J. B., Mauldin, R. L., Eisele, F. L., and Kosciuch, E.: CIMS measurements of HNO_3 and SO_2 at the south pole during ISCAT 2000, Atmos. Environ., 38, 5411–5421, 2004.

Huey, L. G.: Measurement of trace atmospheric species by chemical ionization mass spectrometry: Speciation of reactive nitrogen and future directions, Mass Spectrom. Rev, 26, 166–184, 2007.

JPL 06-2: Chemical Kinetics and Photochemical Data for Use in Atmospheric Studies Evaluation Number 15, National Aeronautics and Space Administration, Jet Propulsion Laboratory, California Institute of Technology, Pasadena, CA, USA, 2006.

Kajino, M., Ueda, H., and Nakayama, S.: Secondary acidification: Changes in gas-aerosol partitioning of semivolatile nitric acid and enhancement of its deposition due to increased emission and concentration of SO_x, J. Geophys. Res., 113, D03302, doi:10.1029/2007JD008635, 2008.

Karagulian, F., and Rossi, M. J.: Heterogeneous chemistry of the no3 free radical and n2o5 on decane flame soot at ambient temperature: Reaction products and kinetics, J. Phys. Chem. A, 111, 1914–1926, 2007.

Lei, W., de Foy, B., Zavala, M., Volkamer, R., and Molina, L. T.: Characterizing ozone production in the Mexico City metropolitan area: A case study using a chemical transport model, Atmos. Chem. Phys., 7, 1347–1366, 2007, http://www.atmos-chem-phys.net/7/1347/2007/.

Lei, W., Zhang, R., McGivern, W. S., Derecskei-Kovacs, A., and North, S. W.: Theoretical study of isomeric branching in the isoprene-OH reaction: Implications to final product yields in Isoprene Oxidation, Chem. Phys. Lett., 326, 109–114, 2000.

Lei, W. F., Zhang, R. Y., Tie, X. X., and Hess, P.: Chemical charac-

terization of ozone formation in the Houston-Galveston area: A chemical transport model study, J. Geophys. Res.-Atmos., 109, D12301, doi:10.1029/2003JD004219, 2004.

Maring, H., Savoie, D. L., Izaguirre, M. A., Custals, L., and Reid, J. S.: Mineral dust aerosol size distribution change during atmospheric transport, J. Geophys. Res.-Atmos., 108(D19), 8592, doi:10.1029/2002JD002536, 2003.

Mason, E. A. and McDaniel, E. W.: Transport properties of ions in gases, Wiley, New York, USA, xvi, 560 pp., 1988.

Molina, L. T. and Molina, M. J.: Air quality in the Mexico megacity: An integrated assessment, Alliance for global sustainability book series, 2, Kluwer Academic Publishers, Dordrecht, The Netherlands, Boston, USA, xxi, 384 pp., 2002.

Molina, M. J. and Molina, L. T.: Megacities and atmospheric pollution, J. Air Waste Ma., 54, 644–680, 2004.

Molina, L. T., Kolb, C. E., de Foy, B., Lamb, B. K., Brune, W. H., Jimenez, J. L., Ramos-Villegas, R., Sarmiento, J., Paramo-Figueroa, V. H., Cardenas, B., Gutierrez-Avedoy, V., and Molina, M. J.: Air quality in north America's most populous city – overview of the MCMA-2003 campaign, Atmos. Chem. Phys., 7, 2447–2473, 2007, http://www.atmos-chem-phys.net/7/2447/2007/.

Molina, L. T., Madronich, S., Gaffney, J. S., Singh, H. B.: Overview of MILAGRO/INTEX-B Campaign, IGAC Newsletter, Issue No. 38, 2–15, April 2008.

Moya, M., Grutter, M., and Baez, A.: Diurnal variability of size-differentiated inorganic aerosols and their gas-phase precursors during January and February of 2003 near downtown Mexico City, Atmos. Environ., 38, 5651–5661, 2004.

Myles, L., Meyers, T. P., and Robinson, L.: Relaxed eddy accumulation measurements of ammonia, nitric acid, sulfur dioxide and particulate sulfate dry deposition near Tampa, FL, USA, Environ. Res. Lett. 2, 034004, doi:10.1088/1748-9326/2/3/034004, 2007.

Neuman, J. A., Huey, L. G., Ryerson, T. B., and Fahey, D. W.: Study of inlet materials for sampling atmospheric nitric acid, Environ. Sci. Technol., 33, 1133–1136, 1999.

Okumura, M. and Sander, S. P.: Gas-Phase Formation Rates of Nitric Acid and its Isomers under Urban Conditions – Final Report to California Air Resources Board, CARB Contract No. 03-333, 21 November 2005.

Perrino, C., Desantis, F., and Febo, A.: Criteria for the choice of a denuder sampling technique devoted to the measurement of atmospheric nitrous and nitric-acids, Atmos. Environ. a-Gen., 24, 617–626, 1990.

Pryor, S. C. and Klemm, O.: Experimentally derived estimates of nitric acid dry deposition velocity and viscous sub-layer resistance at a conifer forest. Atmos. Environ., 38, 2769–2777, 2004.

Querol, X., Pey, J., Minguillón, M. C., Pérez, N., Alastuey, A., Viana, M., Moreno, T., Bernabé, R. M., Blanco, S., Cárdenas, B., Vega, E., Sosa, G., Escalona, S., Ruiz, H., and Artíñano, B.: PM speciation and sources in Mexico during the MILAGRO-2006 Campaign, Atmos. Chem. Phys., 8, 111–128, 2008, http://www.atmos-chem-phys.net/8/111/2008/.

Ramazan, K. A., Wingen, L. M., Miller, Y., Chaban, G. M., Gerber, R. B., Xantheas, S. S., and Finlayson-Pitts, B. J.: New experimental and theoretical approach to the heterogeneous hydrolysis of no2: Key role of molecular nitric acid and its complexes, J. Phys. Chem. A, 110, 6886–6897, doi:10.1021/Jp056426n, 2006.

Salcedo, D., Onasch, T. B., Dzepina, K., Canagaratna, M. R., Zhang, Q., Huffman, J. A., DeCarlo, P. F., Jayne, J. T., Mortimer, P., Worsnop, D. R., Kolb, C. E., Johnson, K. S., Zuberi, B., Marr, L. C., Volkamer, R., Molina, L. T., Molina, M. J., Cardenas, B., Bernabe, R. M., Marquez, C., Gaffney, J. S., Marley, N. A., Laskin, A., Shutthanandan, V., Xie, Y., Brune, W., Lesher, R., Shirley, T., and Jimenez, J. L.: Characterization of ambient aerosols in Mexico City during the MCMA-2003 campaign with aerosol mass spectrometry: Results from the CENICA supersite, Atmos. Chem. Phys., 6, 925–946, 2006, http://www.atmos-chem-phys.net/6/925/2006/.

Saliba, N. A., Yang, H., and Finlayson-Pitts, B. J.: Reaction of gaseous nitric oxide with nitric acid on silica surfaces in the presence of water at room temperature, J. Phys. Chem. A, 105, 10 339–10 346, doi:10.1021/Jp012330r, 2001.

Seinfeld, J. H. and Pandis, S. N.: Atmospheric Chemistry and Physics: From Air Pollution to Climate Change, Wiley, New York, USA, xxvii, 1326 pp., 1998.

Sillman, S.: The relation between ozone, nox and hydrocarbons in urban and polluted rural environments, Atmos. Environ., 33, 1821–1845, 1999.

Simon, P. K. and Dasgupta, P. K.: Continuous automated measurement of gaseous nitrous and nitric-acids and particulate nitrite and nitrate, Environ. Sci. Technol., 29, 1534–1541, 1995.

Slusher, D. L., Huey, L. G., Tanner, D. J., Flocke, F. M., and Roberts, J. M.: A thermal dissociation-chemical ionization mass spectrometry (TD-CIMS) technique for the simultaneous measurement of peroxyacyl nitrates and dinitrogen pentoxide, J. Geophys. Res.-Atmos., 109, D19315, 2004.

Stutz, J., Alicke, B., Ackermann, R., Geyer, A., White, A., and Williams, E.: Vertical profiles of no3, n2o5, o-3, and nox in the nocturnal boundary layer: 1. Observations during the Texas air quality study 2000, J. Geophys. Res.-Atmos., 109, D12306, doi:10.1029/2003JD004209, 2004.

Suh, I., Lei, W. F., and Zhang, R. Y.: Experimental and theoretical studies of isoprene reaction with NO_3, J. Phys. Chem. A, 105, 6471–6478, 2001.

Suh, I., Zhang, D., Zhang, R., Molina, L. T., and Molina, M. J.: Theoretical study of OH addition to toluene, Chem. Phys. Lett., 364, 454–462, 2002.

Suh, I., Zhang, R., Molina, L. T., and Molina, M. J.: Oxidation mechanism of aromatic peroxy and bicyclic radicals from OH-toluene reactions, J. Am. Chem. Soc., 125, 12 655–12 665, 2003.

Talbot, R. W., Vijgen, A. S., and Harriss, R. C.: Measuring tropospheric HNO_3 – problems and prospects for nylon filter and mist chamber techniques, J. Geophys. Res.-Atmos., 95, 7553–7561, 1990.

Tie, X., Zhang, R., Brasseur, G., Emmons, L., and Lei, W.: Effects of lightning on reactive nitrogen and nitrogen reservoir species, J. Geophys. Res., 106, 3167–3178, 2001.

Tie, X. X., Madronich, S., Li, G. H., Ying, Z. M., Zhang, R., Garcia, A. R., Lee-Taylor, J., and Liu, Y. B.: Characterizations of chemical oxidants in Mexico City: A regional chemical dynamical model (WRF-CHEM) study, Atmos. Environ., 41, 1989-2008, 2007.

Viehland, L. A., Mason, E. A., Morrison, W. F., and Flannery, M. R.: Tables of transport collision integrals for (n, 6, 4) ion-neutral potentials, Atom Data Nucl Data, 16, 495–514, 1975.

Volkamer, R., Jimenez, J. L., San Martini, F., Dzepina, K., Zhang, Q., Salcedo, D., Molina, L. T., Worsnop, D. R., and Molina, M.

J.: Secondary Organic Aerosol Formation from Anthropogenic Air Pollution: Rapid and Higher than Expected, Geophys. Res.. Lett., 33(17), L17811, doi:10.1029/2006GL026899, 2006.

Volkamer, R., Sheehy, P. M., Molina, L. T., and Molina, M. J.: Oxidative capacity of the Mexico City atmosphere – Part 1: A radical source perspective, Atmos. Chem. Phys. Discuss., 7, 5365–5412, 2007, http://www.atmos-chem-phys-discuss.net/7/5365/2007/.

Zhang, D., Zhang, R., Park, J., and North, S. W.: Hydroxy peroxy nitrites and nitrates from OH initiated reactions of isoprene, J. Am. Chem. Soc., 124, 9600–9605, 2002.

Zhang, R., Leu, M. T., and Keyser, L. F.: Hydrolysis of N_2O_5 and $ClONO_2$ on the $H_2SO_4/HNO_3/H_2O$ ternary solutions under stratospheric conditions, Geophys. Res. Lett., 22, 1493–1496, 1995.

Zhang, R., Tie, X., and Bond, D. W.: Impacts of anthropogenic and natural NO_x sources over the US on tropospheric chemistry, P. Natl. Acad. Sci. USA, 100, 1505–1509, 2003.

Zhang, R. Y., Lei, W. F., Tie, X. X., and Hess, P.: Industrial emissions cause extreme urban ozone diurnal variability, P. Natl. Acad. Sci. USA, 101, 6346–6350, 2004a.

Zhang, R. Y., Suh, I., Zhao, J., Zhang, D., Fortner, E. C., Tie, X. X., Molina, L. T., and Molina, M. J.: Atmospheric new particle formation enhanced by organic acids, Science, 304, 1487–1490, 2004b.

Zhao, J. and Zhang, R. Y.: Proton transfer reaction rate constants between hydronium ion ($H_3O^{(+)}$) and volatile organic compounds, Atmos. Environ., 38, 2177–2185, 2004a.

Zhao, J., Zhang, R., Fortner, E. C., and North, S. W.: Quantification of hydroxycarbonyls from OH-isoprene reactions, J. Am. Chem. Soc., 126, 2686–2687, 2004b.